Low Computational Burden Predictive Direct Power Control of Quasi Z-Source Inverter for Grid-Tied PV Applications

Abid, Abderahmane; Bakeer, Abualkasim; Zellouma, Laid ; Bouzidi , Mansour; Lashab, Abderezak; Rabhi, Boualaga

Published in:
Sustainability

DOI (link to publication from Publisher):
10.3390/su15054153

Publication date:
2023

Document Version
Publisher's PDF, also known as Version of record

sustainability

MDPI

Article

Low Computational Burden Predictive Direct Power Control of Quasi Z-Source Inverter for Grid-Tied PV Applications

Abderahmane Abid [1,*], Abualkasim Bakeer [2,*], Laid Zellouma [1], Mansour Bouzidi [3], Abderezak Lashab [4] and Boualaga Rabhi [5]

[1] LEVRES Laboratory, Department of Electrical Engineering, El-Oued University, El-Oued 3900, Algeria
[2] Department of Electrical Engineering, Faculty of Engineering, Aswan University, Aswan 81542, Egypt
[3] Department of Electronics and Communications, Ouargla University, Ouargla 30000, Algeria
[4] Center for Research on Microgrids (CROM), Aalborg University, 9220 Aalborg, Denmark
[5] Department of Electrical Engineering, Biskra University, Biskra 7000, Algeria
* Correspondence: abderahmane30@gmail.com (A.A.); abualkasim.bakeer@aswu.edu.eg (A.B.)

Abstract: This paper proposes a simplified predictive direct power control for the grid-tied quasi Z-source inverter. The proposed control implements a model predictive control structure to achieve the maximum obtainable power from the collected PV source. The power delivered to the grid is managed to compensate for the reactive power and, as needed, to ensure the grid's stability. A predictive power model for a quasi Z-source inverter is developed in which the proposed control can operate with a fixed switching frequency without a weighting factor. The simplified space vector modulation uses the three appropriate switching vectors that are selected and applied using precalculated switching times during each switching period, in which the required switching vectors are determined only from one sector in the space vector diagram, taking all of the information of the other sectors, which leads to reducing the computational burden. Simulation results and comparative study are used to confirm the proposed control performance for the grid-tied quasi Z-source inverter capable of tracking and generating the maximum power from PV with fast-tracking dynamics, ensuring the ac voltage desired, and better tracking of the active and reactive power reference with the lowest power ripple. The grid current harmonics were tested and conformed to the IEEE-519 standard. Additionally, the proposed simplified PDPC is experimentally validated using the Hardware-in-the-Loop emulator and the C2000TM-microcontroller-LaunchPadXL TMS320F28379D kit, establishing the usability and good result of our proposed control approach in terms of requirements.

Keywords: distributed generation; model predictive control; photovoltaic source; space vector modulation; switching frequency; switching times; hardware-in-the-loop (HIL)

Citation: Abid, A.; Bakeer, A.; Zellouma, L.; Bouzidi, M.; Lashab, A.; Rabhi, B. Low Computational Burden Predictive Direct Power Control of Quasi Z-Source Inverter for Grid-Tied PV Applications. *Sustainability* **2023**, *15*, 4153. https://doi.org/10.3390/su15054153

Academic Editors: Andrii Chub, Mohamed Trabelsi and Sertac Bayhan

Received: 9 January 2023
Revised: 21 February 2023
Accepted: 22 February 2023
Published: 24 February 2023

1. Introduction

The global installed photovoltaic (PV) power capacity is increasing nearly exponentially as costs fall and solar energy technology improves. According to the International Energy Agency (IEA), solar PV generation will exceed 1000 TWh in 2021 by a register of 179 TWh (up 22%) and in 2030, solar PV generation will have increased to a level of around 7400 TWh annually [1]. PV cells, on the other hand, generate lower direct current (dc) voltage when compared to the high-voltage alternating current (ac) grid, necessitating the utilization of a power electronics converter for step-up by dc/dc or dc/ac conversion, which requires the maximum power point tracking (MPPT) technique for optimum functioning [2,3].

In addition, it generally necessitates the use of several power converter stages. Many familiar PV inverter topologies were two staged with an energy storage element, such as a dc-link capacitor [4,5]. Conventional PV energy extracting systems need a dc/dc stage for boosting and a dc/ac converter for inversion quality [5]. The two-staged system's efficiency and dynamic behavior are decreased due to changes in the external environment

and grid disturbances. Furthermore, the inverter needs to provide a smart-grid interface and improve inverter capabilities. As a result, the ideal distributed generation (DG) requires the power electronics interface (PEI) of the conversion stage for a highly efficient, comprehensive, and suitable controller for grid integration.

Various strategies for PV single-stage grid integration have been explored, in which the inverter achieves the tracking of the optimum power, voltage boosting, and inversion capabilities [6,7]. The Z-source inverter (ZSI) and quasi Z-source inverter (qZSI) have been studied widely for PV applications due to their capacity to buck or boost the dc input voltage by connecting an impedance network between the power generator and the inverter port [8]. The ZSI/qZSI can offer a more challenging, efficient, reliable, and competitively priced approach with a single-stage conversion and a lower number of active switching devices [9]. Due to these characteristics, RES can use ZSI/qZSI to overcome the drawbacks of voltage source inverter (VSI) topologies [10]. Recently suggested qZSI got some new appealing advantages that make them more beneficial for PV systems [11]. The qZSI has a continuous input current, which eliminates electromagnetic interference and leakage/ground current flow while enhancing PV lifetime and energy production [12]. Moreover, the voltage between one of the two capacitors in the impedance network is lesser than the voltage across to the other capacitor, allowing for lower rating capacitors, which can decrease the cost, in contrast to the situation in ZSI [13,14].

The control strategy is essential since it heavily influences the performance of the grid-connected inverter and thus enhances the grid power quality. As a result, grid- connected control research has focused on controlling strategy [5,15]. Various qZSI control methods, particularly linear and nonlinear control concepts, have been presented in the literature in a synchronous, stationary, or natural frame [16]. Furthermore, the performance of the aforementioned control methods is highly dependent on the quality of the inner current loop due to the proportional-integral (PI) controller, which requires a decoupling that appears to be complex. Moreover, the PI controller cannot obtain an error-free adjustment [17], as well as the bandwidth of the phase-locked loop (PLL) for synchronization [18]. Direct power control (DPC) is mainly investigated due to its simplicity of application, low current distortion levels, and dynamic performance [19]. A traditional DPC structure typically employs a power hysteresis comparator and a switching vector table to choose a voltage vector. The active and reactive powers are directly controlled without using an inner current control circuit or a pulse width modulation (PWM) block [20]. The implementation of hysteresis comparators for power control generates high-power ripples and variable switching frequency, which increase the power losses and produces an unexpected wide band gap harmonic spectrum range, which implies that designing a line filter is difficult. Model predictive control (MPC) has become a popular technique for power converters in the last decade due to its simplicity, flexibility, and ease of adding control limitations [21–25].

The decoupling between the active and reactive power predictive control is presented in [26]. However, this method requires the addition of three weighting factors to the cost function, which can lead to an increase in the output power ripple. In [27], the improvement of the MPPT algorithm in the model predictive can enhance the output current quality, however, the model is more complex. Model predictive control of dual-mode operations for the Z-Source inverter is proposed in [28] and presented when the algorithm works in the double function, however, the switching frequency is not fixed. The authors of [29] proposed the model predictive power control without weighting factors for reducing the computational burden, though the power ripple is still significant.

Nevertheless, despite these benefits of the traditional MPC, three significant limitations are reducing its effectiveness [19–23]. The first drawback is the variable switching frequency, which causes a huge current ripple and complicates designing filters. The second shortcoming is the complication of the weighting factor selection, which generally depends on a trial-and-error procedure with thorough theory instructions [30,31]. The last disadvantage is that the traditional MPC searches for the best vector using continuous optimization, making it much more computationally costly.

To overcome the mentioned issues with the traditional MPC, the combination of MPC and instantaneous power theory results in a new DPC family known as predictive direct power control (PDPC). Compared to the DPC, the PDPC assures optimal vector selection depending on the power ripple minimization concept using cost function minimization [32]. Furthermore, the predictive power control with space vector modulation (PDPC-SVM) is applied to alleviate the variable frequency of PDPC, as described in [33]. Furthermore, it has a high capability in harmonic current mitigation, power factor correction, and active power injection. Moreover, it works at low switching frequencies [34].

For the qZSI, the shoot-through (*ST*) action should be achieved by simultaneously turning on the upper and lower switches in the same leg of the qZSI. Space vector modulation (ZSVM) and sinusoidal pulse width modulation (ZPWM) are two categories of modulation techniques for the qZSI [35,36]. The *ST* action is embedded into the original zero states in the ZPWM. For example, for the maximum boost control (MBC) [8], is accomplished by comparing the *ST* reference with the carrier signal. Every switching cycle contains only one *ST* vector, which increases the inductor current ripples. For the ZSVM, such as the ZSVM with a six *ST* duration (ZSVM6) strategy [37], the *ST* time is generally equally distributed and then implanted into the switching moment, while the active states remain untouched. The divide of the *ST* time reduces each charge/discharge interval, resulting in smaller inductor current ripples. The ZSVM techniques can be further divided into the following categories [35]: ZSVM based on the *ST* duration divided by one time, two times, four times, and six times, namely ZSVM1, ZSVM2, ZSVM4, and ZSVM6, respectively. In order to reduce the complexity and the computation time, the simplified ZSVM6 for the qZSI was proposed by using only one sector in the voltage space vector to calculate all of the switching sequence for the ZSVM strategy.

This paper proposes a simplified PDPC with a reduced computational burden for grid-tied qZSI without a cost function calculation. This control strategy provides a simple and effective method to select the optimal vector for generating the switching state with a low computational burden. In order to control the active and reactive power injected into the grid, a simplified ZSVM technique is provided for eliminating the weighting factor calculation, where the ST duty ratio is generated based on the PI linear controller, which is fed by an MPPT unit for optimal operation. With the proposed simplified PDPC, not only can the grid-tied qZSI achieve a lower grid current/power ripple, the computation time is also significantly decreased. The rest of this paper is organized as follows. The mathematical model of the qZSI is given in Section 2, while Section 3 discusses the qZSI control structure. The proposed simplified PDPC algorithm, besides the ZSVM of qZSI, is disclosed in detail in Section 4. Section 5 provides illustrations of the simulation results and comparative study. In Section 6, the HIL simulation is applied to demonstrate the benefits of the proposed simplified PDPC technique. Finally, Section 7 presents the conclusion.

2. Grid-Tied qZSI Mathematical Modeling

The topology of the grid-tied qZSI is depicted in Figure 1, in which a quasi Z-source network is directly coupled to the traditional VSI. There are three different switching states for each phase of the grid-tied qZSI: the *P* state, the *O* state, and the *Z* state. The switching mode is described as

$$S_X = \begin{cases} P: \begin{bmatrix} S_{X1}, & S_{X2} \end{bmatrix} = [1,0] \\ O: \begin{bmatrix} S_{X1}, & S_{X2} \end{bmatrix} = [0,1] \\ Z: \begin{bmatrix} S_{X1}, & S_{X2} \end{bmatrix} = [1,1] \end{cases}, X = a,b,c \quad (1)$$

where S_{X1} and S_{X2} represent the upper and lower switch's phase X positions, respectively, the Z state symbolizes the *ST* state, whereas one indicates switching on the switch, while zero means switching it off. The standard grid-connected PV system based on a quasi Z-source network (qZSN) is illustrated in Figure 1. The qZSN contains two inductors L_1, L_2, two capacitors C_1, C_2, a diode D_1, where $L_1 = L_2$ and $C_1 = C_2$.

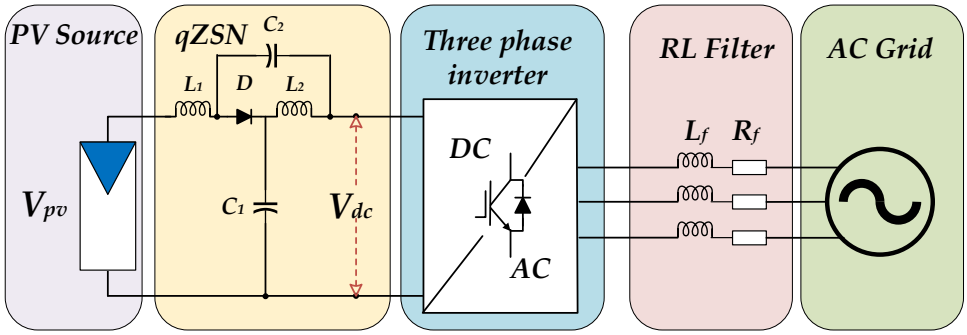

Figure 1. Typical configuration of a grid-connected three-phase qZSI.

The corresponding circuits to both the *ST* state and active one are shown in Figure 2a,b, and it is obvious that there are two operating modes. The first is the *ST* state, in which the dc power and capacitors charge the inductors simultaneously, and the diode is switched off due to negative voltage, as illustrated in Figure 2a. According to Figure 2b, the second is the active mode, when the loads and capacitors are charged by dc power and inductors, where the diode is in forward conduction. In this approach, the inserted *ST* duty ratio value could be utilized to regulate the charging and discharging of the inductors and capacitors, boosting the dc-side voltage without needing an extra boost circuit.

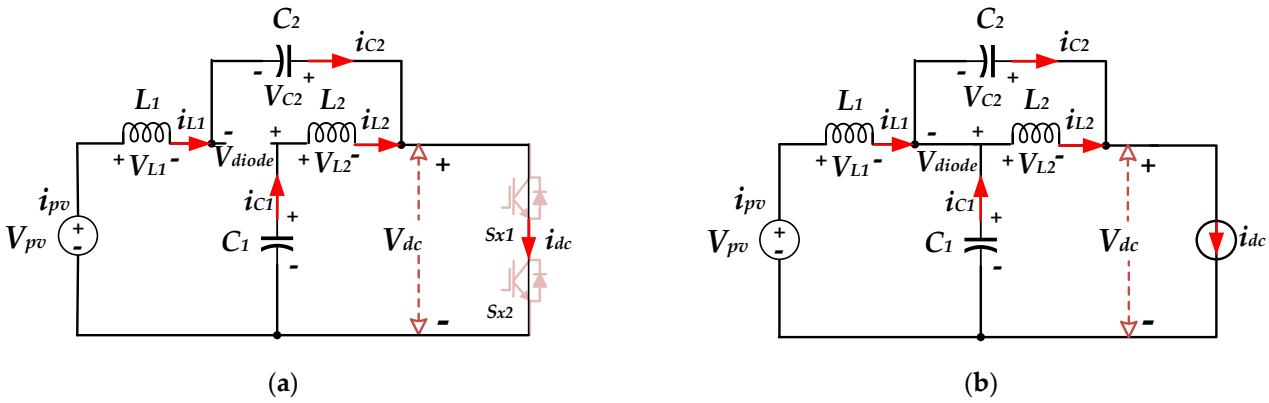

Figure 2. Equivalent qZSI circuits (**a**) *ST* mode and (**b**) active mode.

Referring to [38], depending on the qZSI state space average concept, the average capacitor voltages V_{C1} and V_{C2} can be obtained, respectively, as

$$V_{C1} = \frac{1 - D_{sh}}{1 - 2D_{sh}} V_{PV} \ , \quad V_{C2} = \frac{D_{sh}}{1 - 2D_{sh}} V_{PV} \tag{2}$$

The peak dc-link voltage is given by

$$V_{DC} = V_{C1} + V_{C2} = \frac{1}{1 - 2D_{sh}} V_{PV} = B.V_{PV} \tag{3}$$

where B is the boost factor, $D_{sh} = T_{sh}/T_{Sw}$ is the *ST* duty ratio, T_{sh} is the total *ST* duration, and T_{Sw} is the switching period.

Therefore, the peak output ac voltage of the qZSI can be calculated by

$$V_{AC} = B.M.\frac{V_{PV}}{2} \tag{4}$$

where M represents the modulation ratio.

3. Description of Simplified PDPC Approach

The principal main responsibilities of the control method to the system, as seen in Figure 1, are to integrate the qZSI into the grid and guarantee that the PV system is functioning in MPP. It mainly consists of instantaneous power control, model predictive controller, MPPT control, shoot-through segment ZSVM strategy, and PI regulator. The control structure comprises two parts. The primary is the dc circuit control in the PV source, where the MPPT is applied. In addition, the MPPT unit can generate.

The second part is ac part control, which is based on the control of the injected active and reactive power at the desired value, the proposed simplified PDPC computes the qZSI average voltage vector $V_{\alpha\beta}$ using a predictive control algorithm at each sample time. Therefore, the inputs in the predictive control algorithm are the instantaneous active and reactive power, their reference values, and the grid voltage vector $e_{\alpha\beta}$ (see Figure 3).

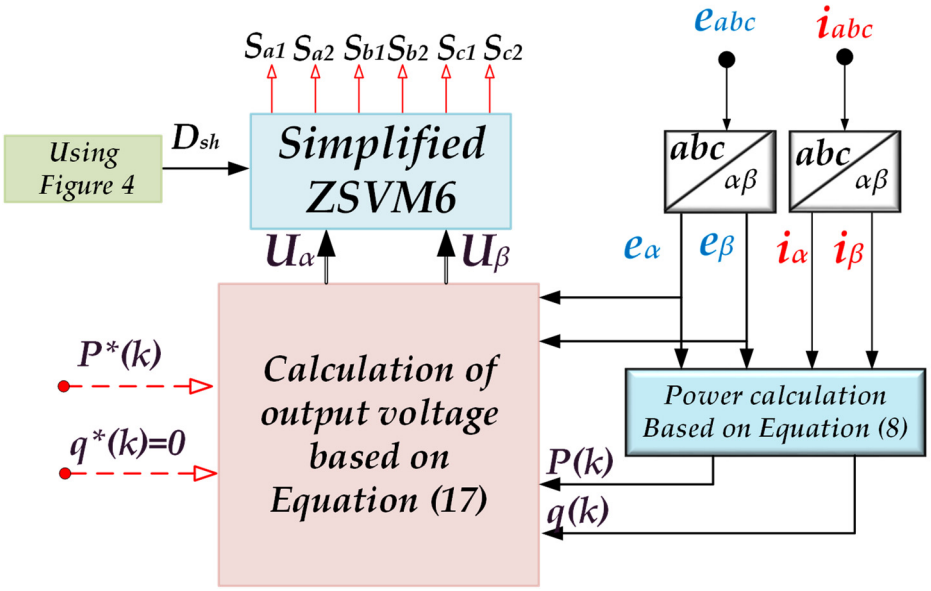

Figure 3. The control diagram of the proposed simplified PDPC.

To operate with a constant switching frequency and low computational time, the ZSVM approach with a simplified algorithm is used to synthesize the average voltage vector $V_{\alpha\beta}$ at the output of the qZSI.

3.1. DC Side Control

In order to generate the *ST* duration, as shown in Figure 4, the perturb and observe method (P&O) is used to achieve the MPPT. The searched maximum power point voltage V_{MPP} is compared with the measured PV array voltage, and the PV voltage closed-loop regulation employs the PI controller to determine the appropriate variety of the *ST* duty ratio for a PV voltage reference adjustment by:

$$D = k_P(V_{PV}^* - V_{PV}) + k_I \int_0^t (V_{PV}^* - V_{PV})dt \tag{5}$$

While the integral and proportional parameters, respectively, are denoted by k_P and k_I. The PV voltage tracking inaccuracy is according to:

$$E = V_{PV}^* - V_{PV} \tag{6}$$

Usually, the transfer function of the PI controller is:

$$G_{PI} = \frac{D}{E} = \frac{k_P p + k_I}{p} \tag{7}$$

The gains k_P and k_I of the PI regulator are determined using the Bode plot approach.

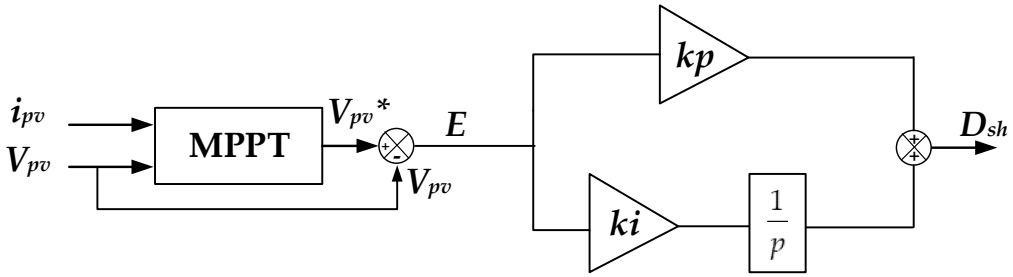

Figure 4. Output PV voltage loop.

3.2. Mathematical Modeling of the PDP

Any prediction system is related to forecasting the control variables to be employed in the sampling period to achieve the desired effectiveness. First, the active and reactive powers will be the controllable variables in the presented prediction model. Both active and reactive power equations in a stationary reference system (α, β), with a balanced three-phase system, are described as follows:

$$\begin{bmatrix} P \\ q \end{bmatrix} = \begin{bmatrix} e_\alpha & e_\beta \\ e_\beta & -e_\alpha \end{bmatrix} \begin{bmatrix} i_\alpha \\ i_\beta \end{bmatrix} \tag{8}$$

When the T_S is supposed to be small in relation to the power-source voltage period, the components of e are considered to be constant across the T_S ($e(k+1) = e(k)$).

Finally, the variation in active and reactive powers during two sequential sampling times can be interpreted as follows:

$$\begin{bmatrix} P(k+1) - P(k) \\ q(k+1) - q(k) \end{bmatrix} = \begin{bmatrix} e_\alpha(k) & e_\beta(k) \\ e_\beta(k) & -e_\alpha(k) \end{bmatrix} \begin{bmatrix} i_\alpha(k+1) - i_\alpha(k) \\ i_\beta(k+1) - i_\beta(k) \end{bmatrix} \tag{9}$$

Figure 1 shows that the qZSI is connected to the grid via an *RL* filter. The system's function at the point of common coupling (PCC) is defined as:

$$V_{abc} = Ri_{abc} + L\frac{di_{abc}}{dt} + e_{abc} \tag{10}$$

where V_{abc} is the output qZSI voltage, i_{abc} is the current injected into the grid through the *RL* filter, and e_{abc} is the PCC voltage. Clarke's transformation of Equation (10) gives:

$$L\frac{d}{dt}\begin{bmatrix} i_\alpha(t) \\ i_\beta(t) \end{bmatrix} = \begin{bmatrix} e_\alpha(t) \\ e_\beta(t) \end{bmatrix} - \begin{bmatrix} V_\alpha \\ V_\beta \end{bmatrix} - R\begin{bmatrix} i_\alpha(t) \\ i_\beta(t) \end{bmatrix} \tag{11}$$

By neglecting the effect of the resistance R_f, the discretization of Equation (11) is given as:

$$\begin{bmatrix} i_\alpha(k+1) - i_\alpha(k) \\ i_\beta(k+1) - i_\beta(k) \end{bmatrix} = \frac{T_S}{L_f}\left(\begin{bmatrix} e_\alpha(k) \\ e_\beta(k) \end{bmatrix} - \begin{bmatrix} V_\alpha(k) \\ V_\beta(k) \end{bmatrix}\right) \tag{12}$$

By replacing Equation (12) in Equation (11), the variation of active and reactive power in one T_S is obtained as follows:

$$\begin{bmatrix} P(k+1) - P(k) \\ q(k+1) - q(k) \end{bmatrix} = \frac{T_S}{L_f}\begin{bmatrix} e_\alpha(k) & e_\beta(k) \\ e_\beta(k) & -e_\alpha(k) \end{bmatrix}\left(\begin{bmatrix} e_\alpha(k) \\ e_\beta(k) \end{bmatrix} - \begin{bmatrix} V_\alpha(k) \\ V_\beta(k) \end{bmatrix}\right) \tag{13}$$

Based on the control objective of PDPC by forcing the active and reactive power to be equal to their reference values at the next sampling instant. Thus,

$$\begin{bmatrix} P(k+1) \\ q(k+1) \end{bmatrix} = \begin{bmatrix} P^*(k+1) \\ q^*(k+1) \end{bmatrix} \tag{14}$$

By substituting Equation (13) in Equation (14), the V_α and V_β reference voltage vectors are calculated as:

$$\begin{bmatrix} V_\alpha(k) \\ V_\beta(k) \end{bmatrix} = \begin{bmatrix} e_\alpha(k) \\ e_\beta(k) \end{bmatrix} - \frac{L_f}{T_S \|e_{\alpha\beta}\|^2} \begin{bmatrix} e_\alpha(k) & e_\beta(k) \\ e_\beta(k) & -e_\alpha(k) \end{bmatrix} \begin{pmatrix} P^*(k+1) - P(k) \\ q^*(k+1) - q(k) \end{pmatrix} \tag{15}$$

To operate at the unity power factor in the grid-tied qZSI, the reactive power reference is equal to zero ($q^* = 0$). As shown in Figure 3, the active power reference (P^*) is achieved by multiplying i_{PV} with V_{PV}. Utilizing the linear approximation shown in Figure 5, the predicted value of $P^*(k + 1)$ is given as follows.

$$\begin{bmatrix} P^*(k+1) \\ q^*(k+1) \end{bmatrix} = \begin{bmatrix} 2P^*(k) - P^*(k-1) \\ q^*(k) \end{bmatrix} \tag{16}$$

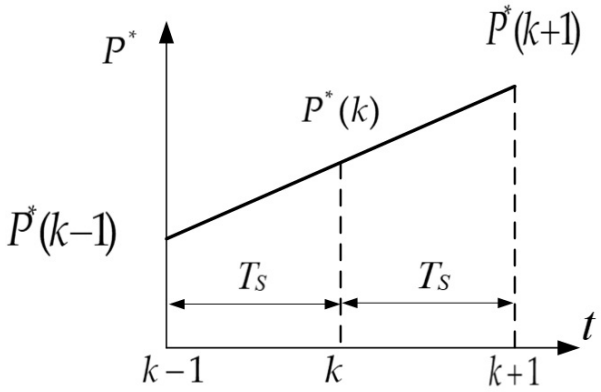

Figure 5. Predictive value estimation of reference active power.

By using Equations (15) and (16), the average control vector to be applied during the sampling period is obtained by the following Equation:

$$\begin{bmatrix} V_\alpha(k) \\ V_\beta(k) \end{bmatrix} = \begin{bmatrix} e_\alpha(k) \\ e_\beta(k) \end{bmatrix} + \frac{L_f}{T_S \|e_{\alpha\beta}\|^2} \begin{bmatrix} e_\alpha(k) & e_\beta(k) \\ e_\beta(k) & -e_\alpha(k) \end{bmatrix} \begin{pmatrix} \Delta P^*(k) + \varepsilon_p(k) \\ \varepsilon_q(k) \end{pmatrix} \tag{17}$$

The actual active and reactive power measuring errors are $\varepsilon_p(k)$ and $\varepsilon_q(k)$, respectively, where $\Delta P^*(k)$ represents the actual variation in active power reference level given by:

$$\Delta P^*(k) = P^*(k) - P^*(k-1) \tag{18}$$

Since the qZSI is supplied by PV panels, the MPPT makes the PV panels deliver their maximum available power repeatedly. The reference power injected into the grid P^* presents the power harvested from the PV panels. The following section describes this modulation technique in more detail.

4. The Simplified Space Vector Modulation

According to Figure 6, the hexagon is divided into six sectors using eight space vectors in the traditional SVM method for the three-phase, two-level VSI. In addition to an extra *ST* zero state, the SVM approach for the qZSI includes all the vectors from the standard SVM strategy. The inverter operation is not affected by the *ST* time of the qZSI since it will

be a section during the zero vector of the traditional SVM approach. The switching time of the sequences in the SVM procedure for the qZSI can be achieved as:

$$\begin{cases} T_1 = M.T_{Sw} \sin[\pi/3 - \theta + (i-1)\pi/3] \\ T_2 = M.T_{Sw} \sin[\theta - (i-1)\pi/3] \\ T_0 = T_{Sw} - T_1 - T_2 \end{cases} \quad (19)$$

where i = 1, 2, . . . , 6 denotes the ith sector, T_{sw} signifies the switching period, T_1 and T_2 represent the durations in time between two neighboring active vectors V_i and V_{i+1}, respectively, T_0 signifies the time interval of the zero vector, which includes the zero vector V_0, and the *ST* vector V_{sh}. V_{ref} denotes the oriented angle of the voltage reference vector the modulation index is defined as $M = \sqrt{3}V_{ref}/V_{DC}$.

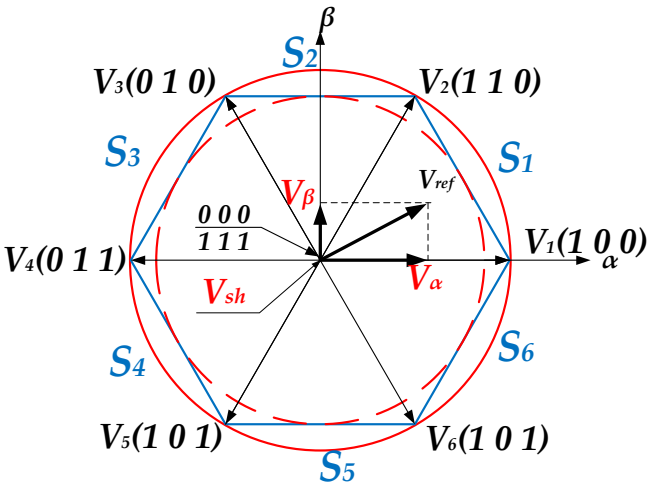

Figure 6. Voltage space vector for ZSVM.

The simplified SVM for the three-phase multilevel inverter was published in [39] to reduce the complexity and the computation time, using only one sector in the voltage space vector to calculate all the switching sequences. The novel simplified ZSVM is proposed to control the grid-tied-qZSI with a low computational time and reduce the hardware and software complexity.

To realize the proposed ZSVM strategy, there are six main steps as the following:

1. New voltage reference vector calculation;
2. Sector number identification;
3. Duration times calculation;
4. Pulses generation with *ST* state insertion.

4.1. Calculations of the New Reference Voltage Vector

To simplify the calculation, the proposed ZSVM algorithm generates a new reference voltage vector $U_{ref} = [U_a, U_b, U_c]^t$ that turns in the first sector and collects all details from the original reference voltage vector $V_{ref} = [V_a, V_b, V_c]^t$ in the other sectors.

In Figure 7, V_{ref} rotates counterclockwise and traverses all sectors of the space vector plan. As a result, the triangle in the first sector is repeated in the remaining sectors.

This similarity is based on the ability to shift the phase directions of the switching states during the first sector to conclude all the switching states for the other sectors. Hence, even if the proposed U_{ref} is only created to rotate in the first sector, the direction of its rotation is also determined by the location of V_{ref}.

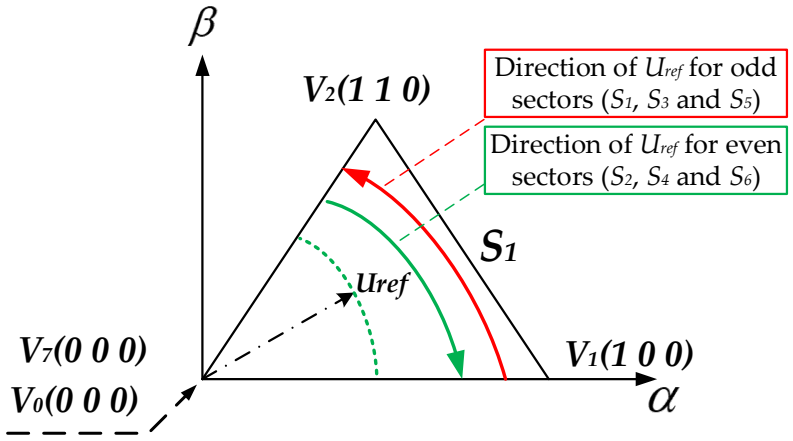

Figure 7. The orientation of the new vector U_{ref} in the first sector.

Assuming that U_{ref} maintains the same triangle order as V_{ref} in all sectors, its rotation must be in the following direction (see Figure 7):

- V_{ref} is in an odd sector (1, 3, and 5) if rotated counterclockwise;
- V_{ref} is in an even sector (2, 4, and 6) if rotated clockwise.

With straightforward instructions, U_{ref} can be generated in the *abc* frame. Table 1 summarizes the selection of the *abc* components of U_{ref}, which depends on V_{ref} components and the number of sectors.

Table 1. Selection of the proposed U_{ref} elements.

	S_1	S_2	S_3	S_4	S_5	S_6
U_a	V_a	V_b	V_b	V_c	V_c	V_a
U_b	V_b	V_a	V_c	V_b	V_a	V_c
U_c	V_c	V_c	V_a	V_a	V_b	V_b

In the *abc* coordinates scheme, Figure 8 depicts the components of the old reference V_{ref} and proposed U_{ref}.

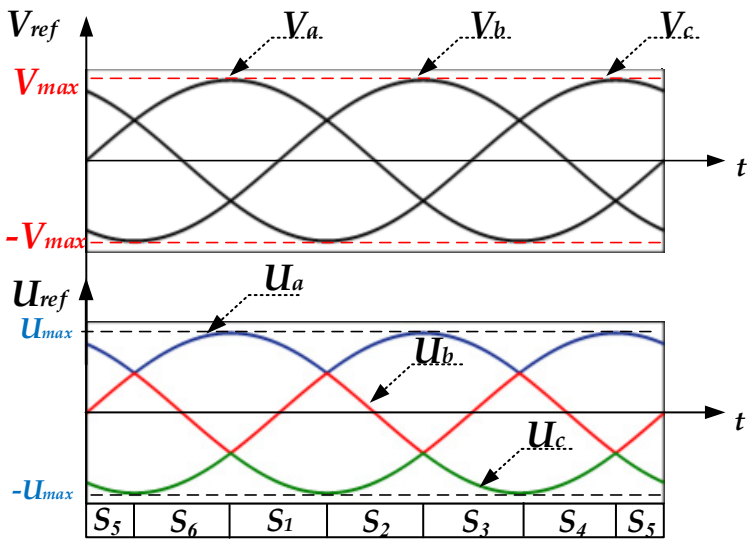

Figure 8. Components of V_{ref} and U_{ref} in abc coordinates.

4.2. Identification of the Sector Number

The sector number containing V_{ref} is required to construct U_{ref}. As a result, Table 2 defines the selected strategy based on an easy comparison of the elements of U_{ref} in abc coordinates.

Table 2. Identification of a sector number.

Condition	Sector Number
$Va > Vb > Vc$	1
$Va > Vc > Vb$	6
$Vb > Va > Vc$	2
$Vb > Vc > Va$	3
$Vc > Vb > Va$	4
$Vc > Va > Vb$	5

4.3. Calculation of Duration Time

To calculate the on-duration time intervals of each switching vector, the average value principle is used and is obtained as follows:

$$\begin{cases} V_1 t_1 + V_2 t_2 + V_0 t_0 = V_{ref} T_{Sw} \\ t_1 + t_2 + t_0 = T_{Sw} \end{cases} \tag{20}$$

where t_1, t_2, and t_0 are the corresponding on-duration time interval for the three switching vectors next to the reference voltage vector, V_1, V_2, and V_0, respectively. Equation (20) is then converted into $\alpha\beta$ coordinates as follows:

$$\begin{bmatrix} V_{1\alpha} & V_{2\alpha} & V_{0\alpha} \\ V_{1\beta} & V_{2\beta} & V_{0\beta} \\ 1 & 1 & 1 \end{bmatrix} \begin{bmatrix} t_1 \\ t_2 \\ t_0 \end{bmatrix} = \begin{bmatrix} V_{\alpha ref} \\ V_{\beta ref} \\ T_{sw} \end{bmatrix} \tag{21}$$

Finally, the on duration can be calculated using Equation (21) based on the voltage reference in $\alpha\beta$ coordinates generated by the PDPC.

4.4. Pulses Generation

The switching operation of the qZSI using the ZSVM includes one additional *ST*, zero vectors, and six active voltage vectors. To create the *ST* state for the ZSVM of qZSI, one of the three-phase legs, *a*, *b*, and *c*, are in a short circuit each switching period. The preferred total *ST* duration is divided into six time during each switching period. One-phase *ST* reduces switching losses across the whole switching period by assuming that only one bridge leg can be altered at a time. Figure 6 shows the corresponding voltage space vectors of the qZSI in an $\alpha\beta$ projection. The switching sequences of the proposed ZSVM6 algorithm in the first sector are detailed in Figure 9 to facilitate switching state selection. Thus, for each sector, the qZSI reference voltage vector becomes:

$$V_{ref} = V_1 \frac{T_1}{T_{Sw}} + V_2 \frac{T_2}{T_{Sw}} + V_0 \frac{T_0}{T_{Sw}} + V_{sh} \frac{T_{sh}}{T_{Sw}} \tag{22}$$

Therefore, the reference voltage is generated using the three adjacent switching vectors. The main objective is to reduce the harmonic content of the output voltage/current by arranging the switching transitions. Table 3 summarizes the adopted interchanging between phases *a*, *b*, and *c* in all sectors.

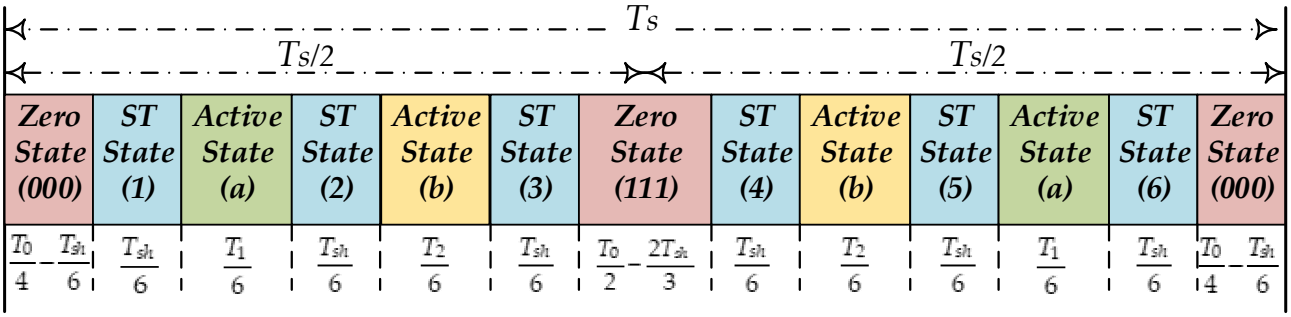

Figure 9. Switching pattern for ZSVM6.

Table 3. Interchanging switching states in all sectors.

Sector 1	Sector 2	Sector 3	Sector 4	Sector 5	Sector 6
a, *b*, *c*	*b*, *a*, *c*	*b*, *c*, *a*	*c*, *b*, *a*	*c*, *a*, *b*	*a*, *c*, *b*

Lastly, Figure 10 shows the flow diagram of the proposed simplified ZSVM6 algorithm for the grid-tied qZSI. The proposed simplified PDPC generates the voltage vector reference V_α and V_β, and utilized Table 2 to create the new U_{ref} for reducing the calculation. The indentation of the sector number is necessary to calculate the vector duration. And to generalize in all sectors, Table 3 illustrates that.

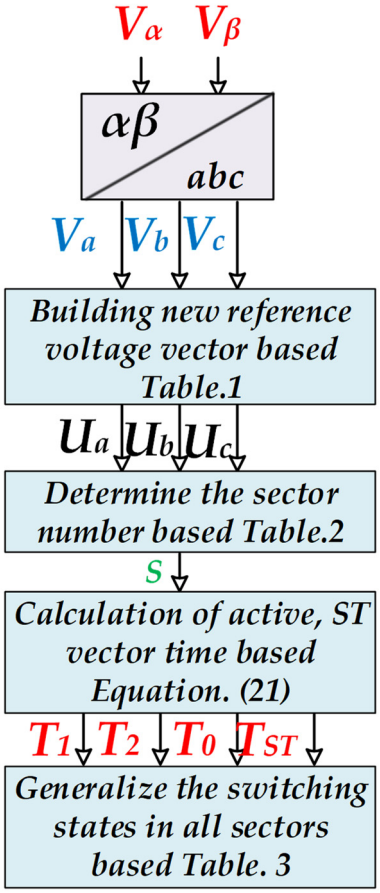

Figure 10. Flow diagram of the proposed simplified ZSVM6.

5. Simulation Results

MATLAB/Simulink is used to simulate the model of the three-phase grid-tied qZSI fed by a PV power system to evaluate the performance of the simplified PDPC method and control structure, as shown in Figure 1. The PV panel's parameters under the standard test conditions (STC) are shown in Table 4. To achieve the required *ac* voltage level, four PV panels were interconnected in a series in each PV string. The electrical system parameters are listed in Table 5. The results are presented in Figures 11–19 and have been validated for the abovementioned criteria.

The system's operation under the dynamic response can be tested under different meteorological conditions. The studied conditions are 1000 W/m^2, 800 W/m^2, and 500 W/m^2, respectively.

As seen in Figure 11, the MPPT operated by P&O precisely follows the theoretical reference. It tracks the maximum voltage with excellent stability and low oscillation. Despite the quick change in irradiation, the panels maintain their maximum output voltage (around 185 V). As seen in Figures 12 and 13, the suggested simplified PDPC can effectively adjust to step variations in the power references, and the maximum output power of the PV source was transferred to the grid with a small active power ripple. As a result, in Figure 14, maintaining reactive power near zero and ensuring that the qZSI is unaffected by changes in active power, allowing the converter to operate at the unity power factor.

Table 4. Photovoltaic module parameters.

Parameter	Value
Maximum power	150 W
Open circuit voltage	22.5 V
Short circuit current	8.75 A
The voltage at the MPP	18.25 V
Currently at the MPP	8.22 A
ΔV (P&O)	0.5 V
Sampling frequency (P&O)	100 Hz

Table 5. System specifications.

Circuit Parameters	Value
qZS network $C_{1,2}$, $L_{1,2}$	1 mF, 4 mH
Internal resistance r_c, R_L	0.19 Ω, 0.1 Ω
Filter inductance L_f, R_f	4 mH, 0.1 Ω
Switching frequency f_{Sw}	10 kHz
Sampling time T_s	10^{-6} s
Input PV voltage	180–185 V
Line frequency f	50 Hz
ac output voltage RMS	110 V

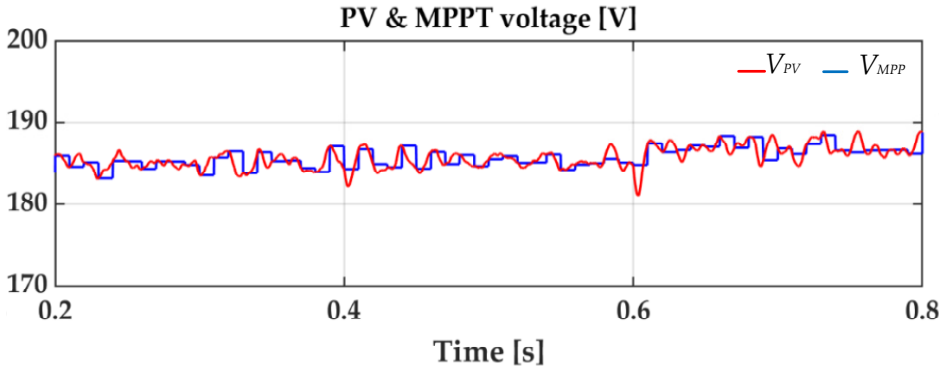

Figure 11. The measured and generated output PV voltage.

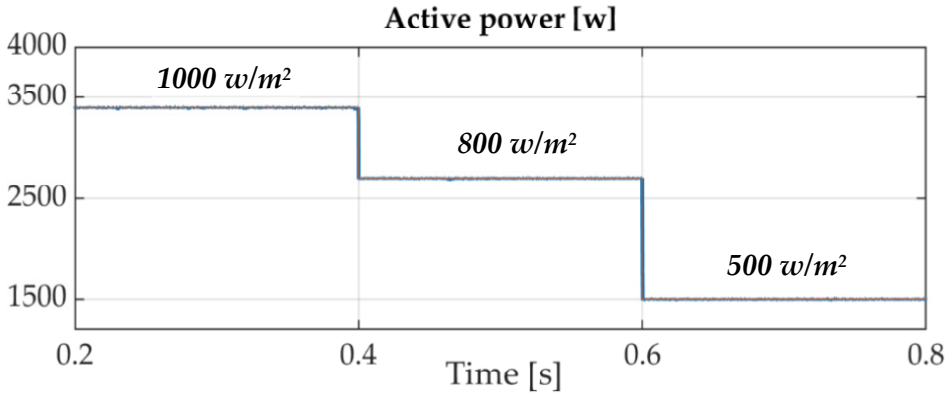

Figure 12. Output active power with a different level of irradiation.

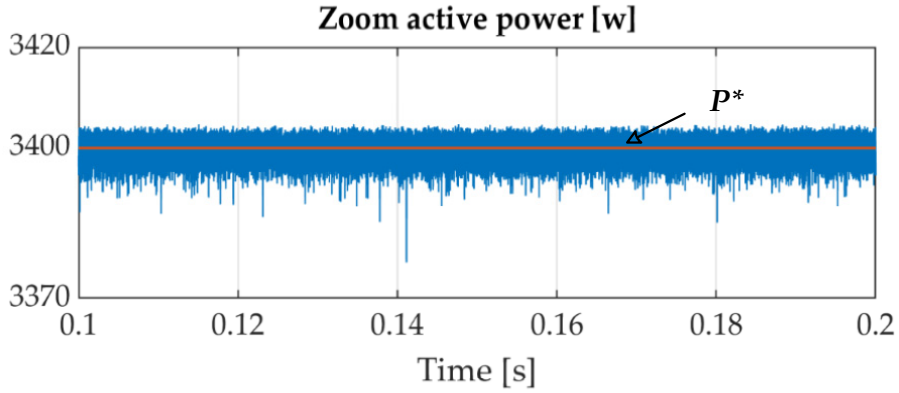

Figure 13. Zoom view in the active output power under 1000 W/m^2.

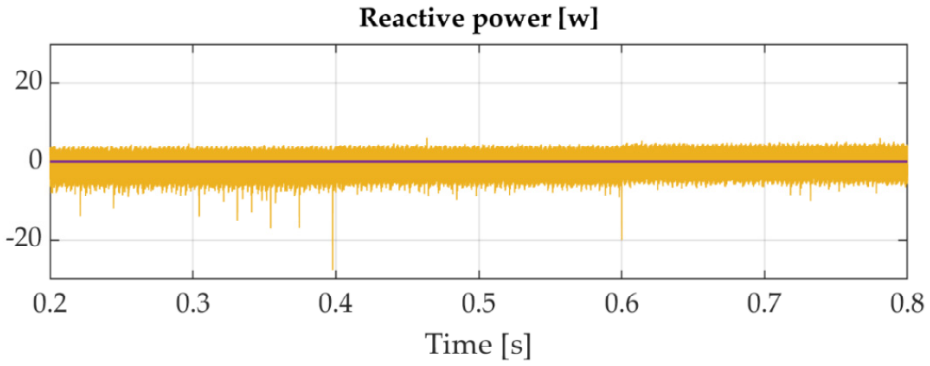

Figure 14. Reactive power under different levels of solar irradiation.

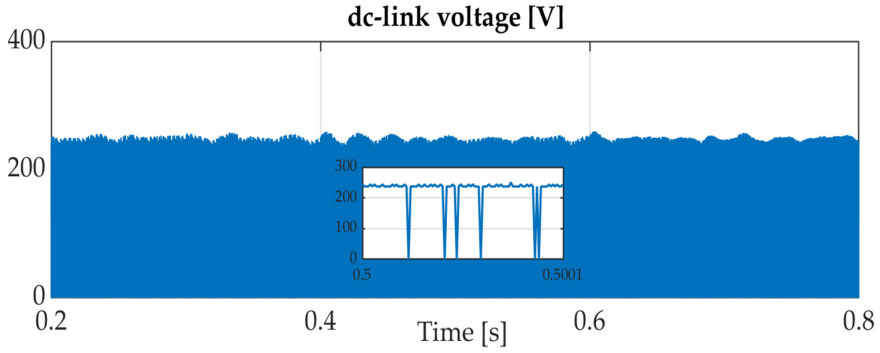

Figure 15. dc-link voltage.

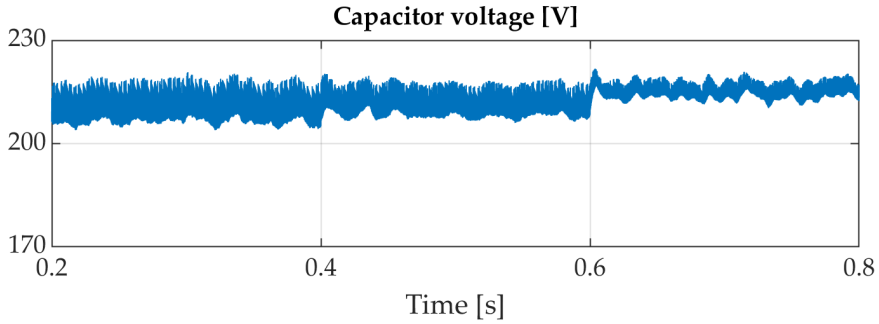

Figure 16. Capacitor C_1 voltage.

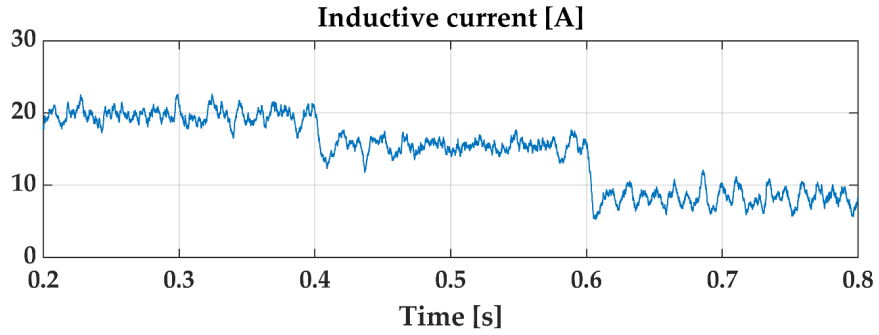

Figure 17. Inductor L_1 current.

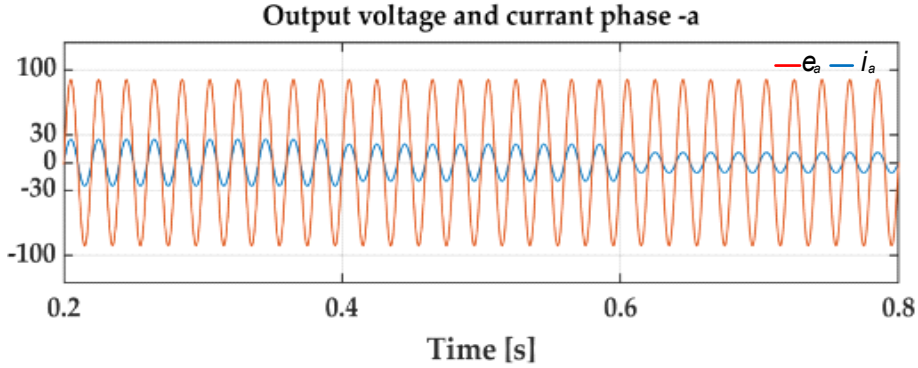

Figure 18. Output voltage and current in phase-*a*.

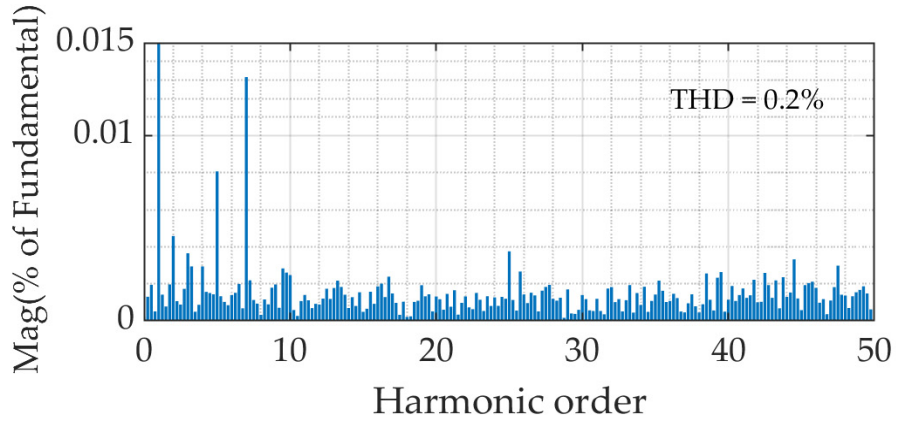

Figure 19. The *a*-phase current spectrum.

It is shown in Figure 15, the *ST* duty cycle is controlled to maintain a dc-link peak voltage value during all the changing in the irradiation and produces a pulse voltage

waveform since, in the *ST* state, the dc-link voltage is zero, while in the active state, the peak dc-link voltage value around 250 V. As shown in Figure 15, the V_{C1} was continuously followed at 220 V during the transient situation, exhibiting the dynamic functionality and efficiency of the proposed control. Figure 17 shows the inductive current waveform during the irradiation changes. It can be seen that the i_{L1} decreases from 20 A to 15 A at 0.4 s and decreases from 15 A to 8 A at 0.6 s. However, we can observe the double frequency comment in the inductive current curve duo to the used one leg for the qZSI for *ST* state. Therefore, the dynamic performance of the qZSI was unaffected by the inductive current ripples.

The V_a and i_a, as presented in Figure 18, are in phase, and the output currents are nearly sinusoidal and fluctuate smoothly. During the irradiation changes, where it can be quickly adjusted without causing overshoot or undershoot currents.

Figure 19 illustrates the grid-tied qZSI's test results in a 1000 W/m^2 steady state, where the current injected into the grid is 20 A RMS with 3.4 kW power. The THD of the injected grid current is 0.2%, which conforms to grid standards IEEE-519 [28]. The waveforms and measurements show that the proposed simplified PDPC is feasible and demonstrates good reference-tracking capabilities.

Table 6 presents a comparative investigation based on the complexity of the model, the output active power ripple, and the line current THD between the proposed simplified PDPC and recently published control schemes [26–29]. The comparison is conducted on the same application, such as grid-connected mode. This comparison demonstrates that the proposed control methods efficiently enhance the line current quality with the Lower ripple in the injected active power.

Table 6. Comparison results between different control strategies.

Reference	Control Used		Modulation	Switching Frequency	Complexity	Power Ripple	THD %
	dc Side	ac Side					
[26]	Model Predictive Current Control With phase lock loop		No need	Variable Average of 22 kHz	High	Medium	3.20%
[27]	Model predictive control		No need	Variable Average of 9 kHz	High	Low	1.92%
[28]	Model predictive control		No need	Variable	High	Low	2.48%
[29]	Dead-beat control	Model Predictive Power Control	Optimal Sector Selection Method	Constant	Medium	Medium	2.27%
Proposed Method	PI controller	Model Predictive Power Control	Simplified space vector modulation	Constant 10 kHz	Low	Low	0.20%

6. HIL Validation Results

A hardware-in-the-loop (HIL) emulator was applied to evaluate and confirm our proposed control scheme for a three-phase grid-tied qZSI. The fundamental elements and signal channels of the HIL simulator for the proposed approach are shown in Figure 20.

In a usual HIL emulator, the three-phase grid-tied qZSI and its various PV irradiation are simulated and conducted on the personal computer (i.e., Host-PC) as a concept in MATLAB. However, the control strategies are carried out in an external target microcontroller kit (in our research, the C2000TM microcontroller-LaunchPadXL TMS320F28379D kit). The HIL emulator necessitates collaboration between the Host-PC and the target LAUNCHXL-F28379D, accomplished through a virtual serial COM port [40,41]. In this case, the Host-PC sends measured signals (or input characteristics) such as V_{pv}, e_{abc}, and i_{abc} to the LAUNCHXL-F28379D kit. After receiving these signals from the target kit, the proposed control strategy designates the switching state for the next switching period. At last, the switching sequences are delivered to the Host-PC to control the qZSI switches and will be repeated at each sampling time T_s.

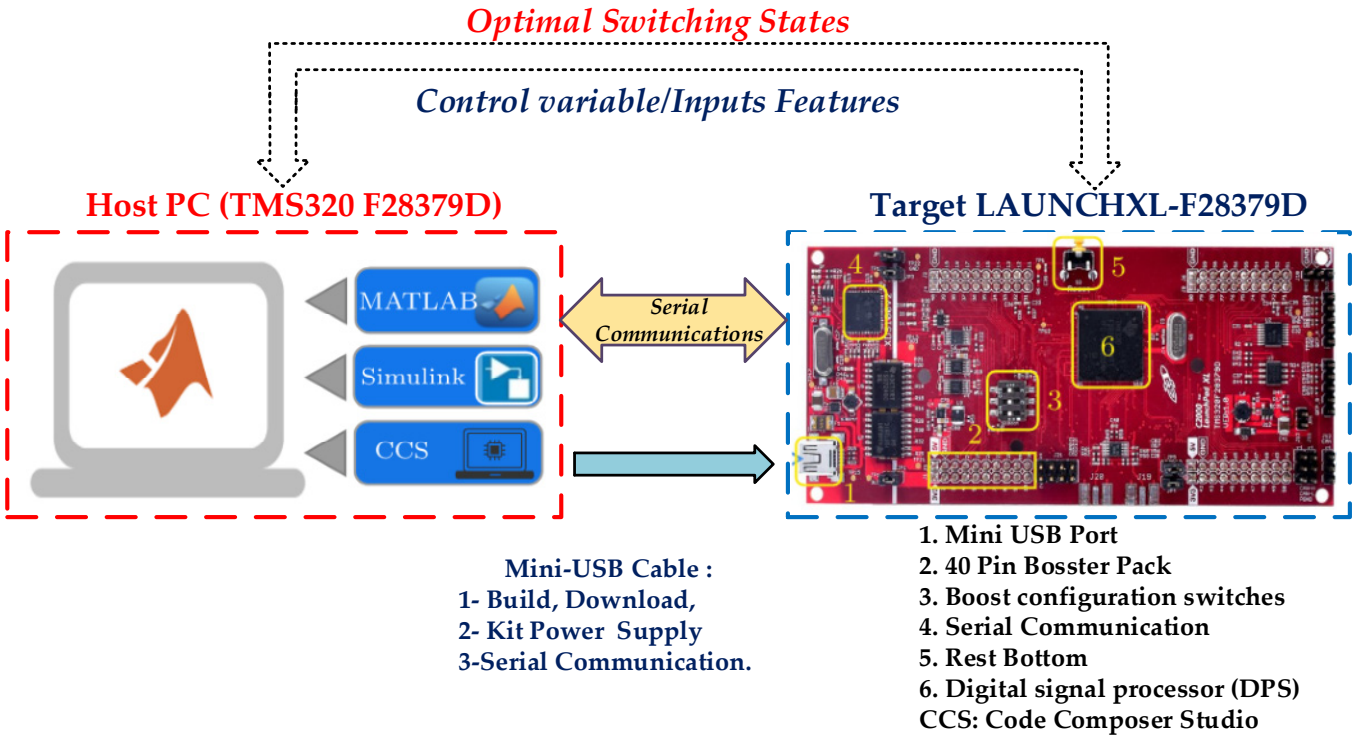

Figure 20. HIL simulator schematic for the proposed system.

After configuring the devices and the Host-PC, as explained in [41], the HIL simulation is used to evaluate the effectiveness of the proposedaa control strategies in controlling the PV output voltage V_{pv}, the active output P, and reactive powers q. The system's operation under the dynamic response can be tested under different meteorological conditions. The studied conditions are 1000 W/m^2 and 800 W/m^2, respectively.

Figures 21 and 22 show the active and reactive powers, and it can be seen that both injected powers track the reference under various solar irradiation.

In Figure 24, the output currents are almost sinusoidal and smoothly fluctuate. Moreover, it can quickly change during irradiation variations without producing overshoot or undershoot currents. Finally, the challenges among simulation and HIL findings are insignificant, demonstrating that the proposed simplified PDPC for grid-tied qZSI is successful in terms of implementations.

It is shown in Figure 23 that maintaining a dc-link peak voltage value through all the changing in the solar irradiation is due to adjusting the *ST* duty cycle.

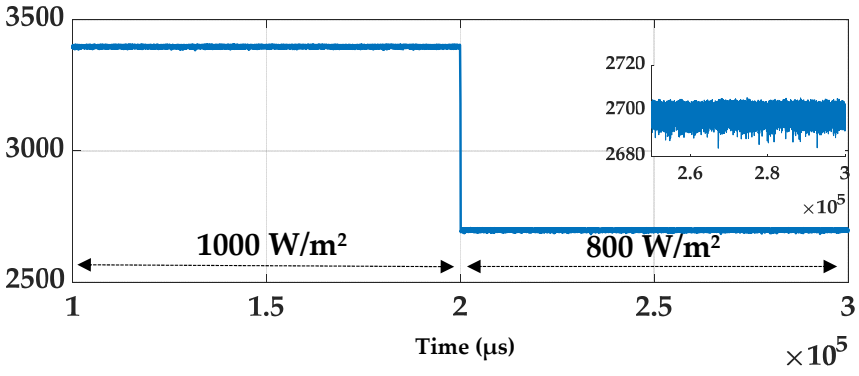

Figure 21. HIL validation: Output active power with a different level of irradiation.

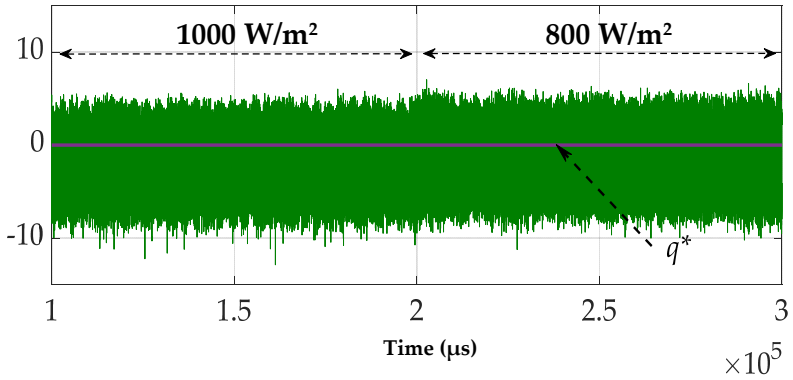

Figure 22. HIL validation: Reactive power under different levels of solar irradiation.

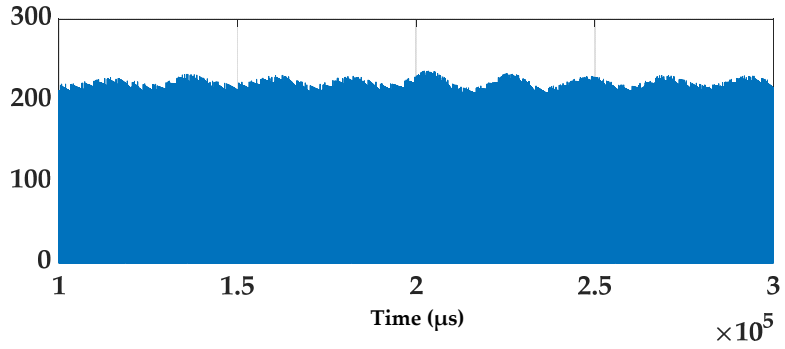

Figure 23. HIL validation: dc-link voltage.

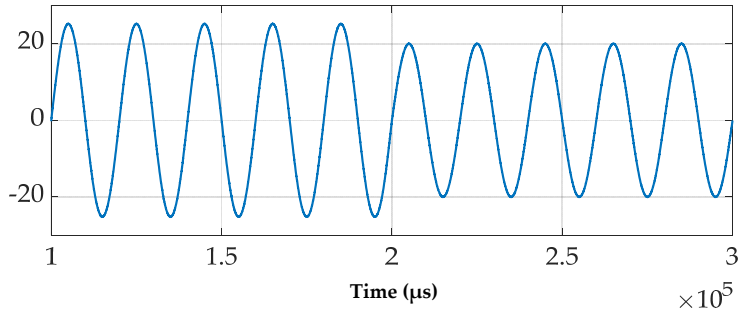

Figure 24. HIL validation: Output current in phase-*a*.

7. Conclusions

This paper proposed a simplified PDPC with a fixed switching frequency for grid-tied qZSI. The suggested control strategy integrates the PDPC approach with the ZSVM block to function at fixed and low switching frequencies, improve system performance, and maintain the durability of its hardware devices. In addition, the simplified ZSVM is based only on the first sector calculation. It uses reference vector identification, *ON*-duration times calculation, and pluses generation with the *ST* state insertion. Consequently, it reduces the calculation time while increasing accuracy. The voltage reference vectors are also computed without the need for linear controllers. A PI controller adjusts the dc link voltage and the traditional P&O algorithm for generating V_{MPP} voltage reference. Finally, the simplified PDPC generates the voltage vector and switching pulses for the qZSI, resulting in the smallest difference between predictive and reference values. The proposed simplified PDPC not only realizes the control of photovoltaic source voltage but also the optimal control of active and reactive powers on the ac side of the qZSI. The obtained results, and comparative evaluation, prove the effectiveness and feasibility of the proposed simplified

PDPC in terms of reached grid *ac* voltage, active and reactive power regulation, and output current quality improvements. The HIL emulator was used to prove its feasibility on a DSP kit and illustrate its performance under varied irradiation levels.

Author Contributions: Conceptualization, A.A.; methodology, A.A., A.B., A.L. and A.B.; software, A.A.; validation, A.A., A.B. and A.L.; formal analysis, A.B.; investigation, A.A. and A.B.; resources, A.A.; data curation, A.A.; writing—original draft preparation, A.A.; writing—review and editing, A.B., L.Z., M.B. and A.L.; visualization, A.B., A.L. and B.R.; supervision, L.Z. and M.B.; project administration, L.Z.; funding acquisition, A.B. and M.B. All authors have read and agreed to the published version of the manuscript.

Funding: This research received no external funding.

Institutional Review Board Statement: Not applicable.

Informed Consent Statement: Not applicable.

Data Availability Statement: The data presented in this study are available on request from the corresponding author.

Conflicts of Interest: The authors declare no conflict of interest.

Nomenclature

MPPT	Maximum power point tracking
ZSI	Z-source inverter
qZSI	Quasi Z-source inverter
VSI	Voltage source inverter
PI	Proportional integral controller
PLL	Phase-locked loop
DPC	Direct power controller
PWM	Pulse width modulation
MPC	Model predictive control
PDPC	Predictive direct power control
SVM	Space vector modulation
MPC	Maximum boost control
ZSVM6	Space vector modulation six *ST* duration
S_{X1}, S_{X2}	States for the upper and lower switch in phase (a, b, c)
L_1, L_2 C_1, C_2	Inductors and capacitors for qZSI (H)
V_{C1}, V_{C2}	Capacitor voltage across C_1, C_2 (V)
D_{sh}	Shoot though duty cycle
B	Boost factor
T_{sh}	Total ST duration (s)
T_{SW}	Switching period (s)
V^*_{pv}, V_{pv}	Measured and reference PV output voltage reference (V)
i_{pv}	Output PV current (A)
P&O	Perturb and observe method
V_{MPP}	Searched maximum power point voltage (V)
K_p, k_I	Proportional and integral constants
E	Error of output PV voltage control loop
G_{PI}	Transfer function of the PI controller
p	Laplace operator
R	Resistance of the filter (Ω)
L	Inductance of the filter (H)
e_a, e_b, e_c	Source voltage of phase a, b, c respectively (V)
V_a, V_b, V_c	Output inverter voltage of phase a, b, c respectively (V)
T_S	Sampling period (s)
P^*, q^*	Reference active and reactive power (w)
r_c, R_L	Internal resistance (Ω)
f	Line frequency (Hz)

References

1. OECD/IEA, IEA (International Energy Agency). Available online: https://www.iea.org/ (accessed on 16 October 2022).
2. Ceglia, F.; Marrasso, E.; Pallotta, G.; Roselli, C.; Sasso, M. The State of the Art of Smart Energy Communities: A Systematic Review of Strengths and Limits. *Energies* **2022**, *15*, 3462. [CrossRef]
3. Kumar, M. Social, Economic, and Environmental Impacts of Renewable Energy Resources. In *Wind Solar Hybrid Renewable Energy System*; Okedu, K.E., Tahour, A., Aissaou, A.G., Eds.; IntechOpen: Rijeka, Croatia, 2020.
4. Kouro, S.; Leon, J.I.; Vinnikov, D.; Franquelo, L.G. Grid-Connected Photovoltaic Systems: An Overview of Recent Research and Emerging PV Converter Technology. *IEEE Ind. Electron. Mag.* **2015**, *9*, 47–61. [CrossRef]
5. Chauhan, A.; Saini, R.P. A Review on Integrated Renewable Energy System Based Power Generation for Stand-Alone Applications: Configurations, Storage Options, Sizing Methodologies and Control. *Renew. Sustain. Energy Rev.* **2014**, *38*, 99–120. [CrossRef]
6. Husev, O.; Vinnikov, D.; Roncero-Clemente, C.; Blaabjerg, F.; Strzelecki, R. MPPT and GMPPT Implementation for Buck-Boost Mode Control of Quasi-Z-Source Inverter. *IEEE Trans. Ind. Electron.* **2022**, *69*, 11348–11358. [CrossRef]
7. Liu, Y.; Abu-Rub, H.; Ge, B.; Blaabjerg, F.; Ellabban, O.; Loh, P.C. Applications in Photovoltaic Power Systems. In *Impedance Source Power Electronic Converters*; Wiley-IEEE Press: Hoboken, NJ, USA, 2016.
8. Liu, Y.; Abu-Rub, H.; Ge, B. Z-Source\/Quasi-Z-Source Inverters: Derived Networks, Modulations, Controls, and Emerging Applications to Photovoltaic Conversion. *IEEE Ind. Electron. Mag.* **2014**, *8*, 32–44. [CrossRef]
9. Abid, A.; Zellouma, L.; Bouzidi, M.; Lashab, A.; Rabhi, B. Switched Inductor Z-Source/Quasi Z-Source Network: State of Art and Challenges. In Proceedings of the 2020 1st International Conference on Communications, Control Systems and Signal Processing (CCSSP), El Oued, Algeria, 16–17 March 2020; IEEE: New York, NY, USA, 2020; pp. 477–482.
10. Li, Y.; Anderson, J.; Peng, F.Z.; Liu, D. Quasi-Z-Source Inverter for Photovoltaic Power Generation Systems. In Proceedings of the 2009 Twenty-Fourth Annual IEEE Applied Power Electronics Conference and Exposition, Washington, WA, USA, 15–19 February 2009; IEEE: New York, NY, USA, 2009; pp. 918–924.
11. Lashab, A.; Sera, D.; Martins, J.; Guerrero, J.M. Dual-Input Quasi-Z-Source PV Inverter: Dynamic Modeling, Design, and Control. *IEEE Trans. Ind. Electron.* **2019**, *67*, 6483–6493. [CrossRef]
12. Monjo, L.; Sainz, L.; Mesas, J.J.; Pedra, J. Quasi-z-Source Inverter-Based Photovoltaic Power System Modeling for Grid Stability Studies. *Energies* **2021**, *14*, 508. [CrossRef]
13. Lashab, A.; Sera, D.; Guerrero, J.M. Model Predictive Control of Cascaded Multilevel Battery Assisted Quasi Z-Source PV Inverter with Reduced Computational Effort. In Proceedings of the 2019 IEEE Energy Conversion Congress and Exposition (ECCE), Baltimore, MD, USA, 29 September–3 October 2019; IEEE: New York, NY, USA, 2019; pp. 6501–6507.
14. Yadav, A.; Chandra, S.; Bajaj, M.; Sharma, N.K.; Ahmed, E.M.; Kamel, S. A Topological Advancement Review of Magnetically Coupled Impedance Source Network Configurations. *Sustainability* **2022**, *14*, 3123. [CrossRef]
15. Grgić, I.; Bašić, M.; Vukadinović, D. Optimization of Electricity Production in a Grid-Tied Solar Power System with a Three-Phase Quasi-Z-Source Inverter. *J. Clean. Prod.* **2019**, *221*, 656–666. [CrossRef]
16. Liang, W.; Liu, Y.; Ge, B.; Li, X.; Ferreira, F.J.T.E.; De Almeida, A.T. Night Operation, Analysis, and Control of Single-Phase Quasi-Z-Source Photovoltaic Power System. *IET Renew. Power Gener.* **2019**, *13*, 2817–2829. [CrossRef]
17. Ellabban, O.; Van Mierlo, J.; Lataire, P. Experimental Study of the Shoot-through Boost Control Methods for the Z-Source Inverter. *EPE J.* **2011**, *21*, 18–29. [CrossRef]
18. Khatibi, M.; Ahmed, S. Z-Source Virtual Synchronous Generator: Operation and Control. In Proceedings of the 2021 IEEE Applied Power Electronics Conference and Exposition (APEC), Virtual, 14–17 June 2021; pp. 97–104. [CrossRef]
19. Yan, S.; Yang, Y.; Hui, S.Y.; Blaabjerg, F. A Review on Direct Power Control of Pulsewidth Modulation Converters. *IEEE Trans. Power Electron.* **2021**, *36*, 11984–12007. [CrossRef]
20. Gui, Y.; Kim, C.; Chung, C.C.; Guerrero, J.M.; Guan, Y.; Vasquez, J.C. Improved Direct Power Control for Grid-Connected Voltage Source Converters. *IEEE Trans. Ind. Electron.* **2018**, *65*, 8041–8051. [CrossRef]
21. Bayhan, S.; Abu-Rub, H.; Balog, R.S. Model Predictive Control of Quasi-Z-Source Four-Leg Inverter. *IEEE Trans. Ind. Electron.* **2016**, *63*, 4506–4516. [CrossRef]
22. Ismeil, M.A.; Bakeer, A.; Orabi, M. Implementation Quasi Z-Source Inverter for PV Applications Based on Finite Control Set-Model Predictive Control. *Int. J. Renew. Energy Res.* **2019**, *9*, 1462–1471.
23. Bakeer, A.; Ismeil, M.A.; Kouzou, A.; Orabi, M. Development of MPC Algorithm for Quasi Z-Source Inverter (QZSI). In Proceedings of the 2015 3rd International Conference on Control, Engineering & Information Technology (CEIT), Tlemcen, Algeria, 25–27 May 2015; IEEE: New York, NY, USA, 2015; pp. 1–6.
24. Bakeer, A.; Ahmed, A.A. Performance Evaluation of PMSM Based on Model Predictive Control with Field Weakening Operation and Bidirectional Quasi Z-Source Inverter. In Proceedings of the 2017 Nineteenth International Middle East Power Systems Conference (MEPCON), Cairo, Egypt, 19–21 December 2017; IEEE: New York, NY, USA, 2017; pp. 741–746.
25. Bakeer, A.; Ismeil, M.A.; Orabi, M. Modified Finite Control Set-Model Predictive Controller (MFCS-MPC) for Quasi z-Source Inverters Based on a Current Observer. *J. Power Electron.* **2017**, *17*, 610–620. [CrossRef]
26. Jain, S.; Shadmand, M.B.; Balog, R.S. Decoupled Active and Reactive Power Predictive Control for PV Applications Using a Grid-Tied Quasi-Z-Source Inverter. *IEEE J. Emerg. Sel. Top. Power Electron.* **2018**, *6*, 1769–1782. [CrossRef]
27. Sajadian, S.; Ahmadi, R.; Zargarzadeh, H. Extremum Seeking-Based Model Predictive MPPT for Grid-Tied Z-Source Inverter for Photovoltaic Systems. *IEEE J. Emerg. Sel. Top. Power Electron.* **2019**, *7*, 216–227. [CrossRef]

28. Sajadian, S.; Ahmadi, R. Model Predictive Control of Dual-Mode Operations Z-Source Inverter: Islanded and Grid-Connected. *IEEE Trans. Power Electron.* **2017**, *33*, 4488–4497. [CrossRef]
29. Duan, X.; Kang, L.; Zhou, H.; Liu, Q. Multivector Model Predictive Power Control with Low Computational Burden for Grid-Tied Quasi-Z-Source Inverter without Weighting Factors. *IEEE Trans. Power Electron.* **2022**, *37*, 11739–11748. [CrossRef]
30. Bakeer, A.; Ismeil, M.A.; Orabi, M. A Powerful Finite Control Set-Model Predictive Control Algorithm for Quasi Z-Source Inverter. *IEEE Trans. Ind. Informatics* **2016**, *12*, 1371–1379. [CrossRef]
31. Bakeer, A.; Magdy, G.; Chub, A.; Vinnikov, D. Predictive Control Based on Ranking Multi-Objective Optimization Approaches for a Quasi-Z Source Inverter. *CSEE J. Power Energy Syst.* **2021**, *7*, 1152–1160. [CrossRef]
32. Bouzidi, M.; Barkat, S.; Krama, A.; Abu-Rub, H. Simplified Predictive Direct Power Control of Three-Phase Three-Level Four-Leg Grid Connected NPC Converter. *IEEE Open J. Ind. Electron. Soc.* **2022**, *3*, 448–459. [CrossRef]
33. Krama, A.; Zellouma, L.; Rabhi, B.; Refaat, S.S.; Bouzidi, M. Real-Time Implementation of High Performance Control Scheme for Grid-Tied PV System for Power Quality Enhancement Based on MPPC-SVM Optimized by PSO Algorithm. *Energies* **2018**, *11*, 3516. [CrossRef]
34. Ouchen, S.; Betka, A.; Abdeddaim, S.; Menadi, A. Fuzzy-Predictive Direct Power Control Implementation of a Grid Connected Photovoltaic System, Associated with an Active Power Filter. *Energy Convers. Manag.* **2016**, *122*, 515–525. [CrossRef]
35. Liu, Y.; Ge, B.; Abu-Rub, H.; Peng, F.Z. Overview of Space Vector Modulations for Three-Phase Z-Source/Quasi-Z-Source Inverters. *IEEE Trans. Power Electron.* **2013**, *29*, 2098–2108. [CrossRef]
36. Abid, A.; Zellouma, L.; Bouzidi, M.; Lashab, A.; Boussabeur, M.T.; Rabhi, B. A Comparative Study of Recent Discontinuous Modulation Techniques for Three-Phase Impedance Source Inverter. In Proceedings of the 13th Seminar on Power Electronics and Control (SEPOC 2021), Virtual, 15–18 May 2021.
37. Liu, W.; Yang, Y.; Kerekes, T.; Vinnikov, D.; Blaabjerg, F. Inductor Current Ripple Analysis and Reduction for Quasi-Z-Source Inverters With an Improved ZSVM6 Strategy. *IEEE Trans. Power Electron.* **2020**, *36*, 7693–7704. [CrossRef]
38. Abdelhakim, A.; Davari, P.; Blaabjerg, F.; Mattavelli, P. Analysis and Design of the Quasi-Z-Source Inverter for Wide Range of Operation. In Proceedings of the 2018 IEEE 19th Workshop on Control and Modeling for Power Electronics (COMPEL), Padova, Italy, 25–28 June 2018. [CrossRef]
39. Bouzidi, M.; Barkat, S.; Krama, A. Simplified Hybrid Space Vector Modulation for Multilevel Diode Clamped Converter. *IET Power Electron.* **2020**, *13*, 3861–3870. [CrossRef]
40. Bakeer, A.; Mohamed, I.S.; Malidarreh, P.B.; Hattabi, I.; Liu, L. An Artificial Neural Network-Based Model Predictive Control for Three-Phase Flying Capacitor Multilevel Inverter. *IEEE Access* **2022**, *10*, 70305–70316. [CrossRef]
41. Zaid, S.A.; Mohamed, I.S.; Bakeer, A.; Liu, L.; Albalawi, H.; Tawfiq, M.E.; Kassem, A.M. From MPC-Based to End-to-End (E2E) Learning-Based Control Policy for Grid-Tied 3L-NPC Transformerless Inverter. *IEEE Access* **2022**, *10*, 57309–57326. [CrossRef]